Preparation and Properties of Poly(methyl Methacrylate)/ Iron Carbonate$_{(p)}$ Nanocomposites

Yi-Chun Chou, C. B. Lin, Hsiao-Yun Yeh

Department of Mechanical and Electro-Mechanical Engineering, Tamkang University, Tamsui, Taipei, Republic of China

Received 20 October 2004; accepted 13 April 2005
DOI 10.1002/app.22433
Published online in Wiley InterScience (www.interscience.wiley.com).

ABSTRACT: The mass transport of methanol mixed with ferric chloride hexahydrate ($FeCl_3 \cdot 6H_2O$) in poly(methyl methacrylate) and poly(methyl methacrylate)/iron carbonate particulate$_{(p)}$ nanocomposites is prepared by chemical vapor crystallization and the resulting materials, which are subjected to characterization to evaluate thermal and optical properties, have been investigated. Mass transport is an anomalous and endothermic process and satisfies the van't Hoff plot. We have prepared successfully poly(methyl methacrylate)(PMMA)/iron carbonate particulates nanocomposites using CO_2 gas slowly diffused into saturated solvent mixture-treated poly(methyl methacrylate) for 48 h. After SEM observation, approximately 80 nm iron carbonate particulates were precipitated and evenly distributed in the poly(methyl methacrylate) matrix. In comparison with solvent mixture-treated PMMA, the cut-off wavelength of transmittance in nanocomposites shifts to the shorter wavelength side (red shift). The presence of nanoscale iron carbonate particulates increased the glass transition temperature of the nanocomposites as determined by differential scanning calorimeter, and the glass transition temperature increased with increasing content of nanoscale iron carbonate particulates. The FTIR spectra of solvent mixture-treated poly(methyl methacrylate) and nanocomposites are also studied. © 2005 Wiley Periodicals, Inc. J Appl Polym Sci 98: 2329–2338, 2005

Key words: synthesis; nanocomposites; diffusion; glass transition; FTIR

INTRODUCTION

Organic solvent transport into thermoplastics is influenced by chemical potential gradient and mechanical stress.[1–3] Mass transport would not stop until chemical potential energy and mechanical stress reach an equilibrium state. According to Alfrey et al.,[4] classifying the behavior of organic solvent transport into thermoplastics accounts for Case I diffusion, Case II diffusion, and anomalous diffusion. The Case I transport is Fickian diffusion, Case II transport is solvent content linear proportional to diffusion time, and anomalous diffusion is a combination of both Case I and Case II diffusions. Organic solvent transport into thermoplastics can decrease the glass transition temperature (T_g)[5] and the sharp front between the section with and without solvent could be observed while the diffusion coefficient changes quickly with solvent concentration.[6] Sarti[7] showed that steps to control the moving velocity of the sharp front are the formation of craze, or crazing. Regions with and without craze have different optical properties, which could give a distinct interface. However, the velocity of the sharp front is irrelevant to swelling stress. Svorcik et al.[8] showed that the polyethylene surface layer has been modified by Fe and Cl ion implantation from $FeCl_3$ water solution at room temperature. This prompted us to investigate the diffusion behavior of methanol mixed with ferric chloride hexahydrate ($FeCl_3 \cdot 6H_2O$) in poly(methyl methacrylate) (PMMA).

Due to the polymer matrix nanocomposites have higher rigidity, strength, and heat-resistance and lower gas permeability and water absorbency than traditional materials; they are popularly used in various industries. Kojima et al.[9] showed that Nylon 6/nanoscale clay composites have higher strength and glass transition temperature (T_g) than a classic Nylon 6. Mano et al.[10] investigated the mechanical behavior of PVC with various concentrations of ferric chloride. Bailey et al.[11] demonstrated the growth mechanism of iron oxide particulates of different morphologies from the forced hydrolysis of ferric chloride solutions. Tawansi et al.[12] analyzed the magnetic properties of PVDF films filled with (x) $FeCl_3$ (20-x) $CoCl_2$, in the mass fraction range of $0\% \leqq x \leqq 20\%$. This mixture of Fe^{3+} and Co^{2+} ions enhanced the magnetoactivity of PVDF. Meanwhile, they suggested that PVC films filled with $MnCl_2$ could be considered good candidates for the one-dimensional magnetic interaction and the calculated magnetic interaction-coupling con-

Correspondence to: C. B. Lin (cblin@mail.tku.edu.tw).
Contract grant sponsor: National Science Council, Taiwan, Republic of China.

stant was found to depend linearly on the $MnCl_2$ filling level.[13]

When a beam of light normally collides with a plane reflector, the reflector length size is longer than the wavelength and these vibrating charges generate spherical scattering waves. These waves would be gathered and form a flat reflect wave, but other reflect waves, on the edge of reflector, still scatter as spherical waves. On the other hand, if the reflector length size is shorter than the wavelength, due to diffraction, reflect waves would become uniform spherical waves.[14] Tyndall[15] showed that the scattering intensity is inversely proportional to visible wavelength with exponent 4 and Rayleigh scattering can demonstrate the Tyndall effect. However, according to our previous study[16] the exponent is smaller than 4 for PMMA after methanol absorption and according to Chou et al.,[17] the exponent is 1.02 to 3.25 for PMMA after methanol mixture $FeCl_3 \cdot 6H_2O$ absorption. The wavelength dependence of scattering intensity is attributed to holes, which are smaller than the visible wavelength, and to cloud. Some researchers[18–21] used scattering theory and the concept of fractals, studying the morphologies or sizes of irregular profiles or gathers. This work is also performed to prepare and characterize PMMA/nanofiller particulate nanocomposites and show their improved thermal and optical properties compared with virgin PMMA.

EXPERIMENTAL

Absorption and desorption study

PMMA was obtained from Nitto Jushi Kogyo, *S*-0 type, in the form of a cast acrylic sheet of 1 mm thickness. Specimens of 20 × 10 × 1 mm were cut from the sheet; specimens were annealed at 90°C in air for 24 h and then furnace cooled to ambient temperature (~30°C).

Ferric chloride hexahydrate ($FeCl_3 \cdot 6H_2O$) and methanol were obtained from Merck and J. T. Baker, respectively. The solvent mixture was prepared with a ratio of $FeCl_3 \cdot 6H_2O$ and methanol at 0.02, 0.05, and 0.08 g/g. Specimens and solvent mixture were preheated separately to the same working temperature. Then each specimen was immersed in the solvent mixture and kept at constant temperature in a thermosatted water bath at 40–60°C. After each experimental interval of exposure, the specimen was removed from the bath, the surface was blotted free of surplus fluid, and its weight was measured, utilizing a ±0.1-mg digital balance. The specimen was quickly returned to the solvent mixture-filled bottle for its next interval of exposure. The specimens were saturated with the solvent mixture at 40–60°C and then desorbed at room temperature for 4 weeks till its weight no longer changed.

Sharp front observation

The sharp front morphology on the cleaved surfaces was observed by a Nikon Co. Optiphot-100 optical microscope (OM). Before the specimen was cleaved, a small depth of groove was made by a sharpened blade and propagated along the groove until the specimen was broken.

Crystallization experiments

The preparation of PMMA matrix nanocomposites was performed by the following method: first, the saturated solvent mixture-treated specimens were mounted on glass rods, which were then fixed to the lid of the crystallization 60°C furnace in a sealed bottle. Crystallization was started by placing a dish with ammonium carbonate [$(NH_4)_2CO_3$]: (Merck) at the bottom of the sealed bottle. Crystallization took place by slow diffusion of CO_2 into the specimens for 48 h, after which the specimens were removed and cleaned. Crystal morphology was observed using a LEO-1530 scanning electron microscope (SEM).

X-ray diffraction

XRD experiments were performed in $\theta/2\theta$ transmission geometry using a Bruker D8A X-ray powder diffractometer and nickel target (1.54, 0.56 Å) to analyze the crystals within the specimen. Data were collected from 10 to 60° 2θ, with a scanning rate 0.1° s^{-1}.

Transmittance study

The transmittance of the specimens was saturated with the solvent mixture and then completely desorbed at ambient temperature and crystallization-treated. Transmittance was measured in the wavelength range of 200–850 nm by a Hitachi U-3410 spectrometer, with a scanning rate 60 nm/min.

Infrared absorption

The specimen from the Fourier-transform infrared (FTIR) spectrometer (Nicolet, AVATAR 320 FTIR) was saturated with solvent mixture and then completely desorbed at ambient temperature and crystallization-treated. The infrared spectrum was measured in the range 650–4000 cm^{-1} by the attenuated total reflectance method using a single-point reflection ATR (attenuated total reflectance, Pike).

DSC analysis

The specimen from the differential scanning calorimeter (DSC) was saturated with solvent mixture and then completely desorbed at ambient temperature and

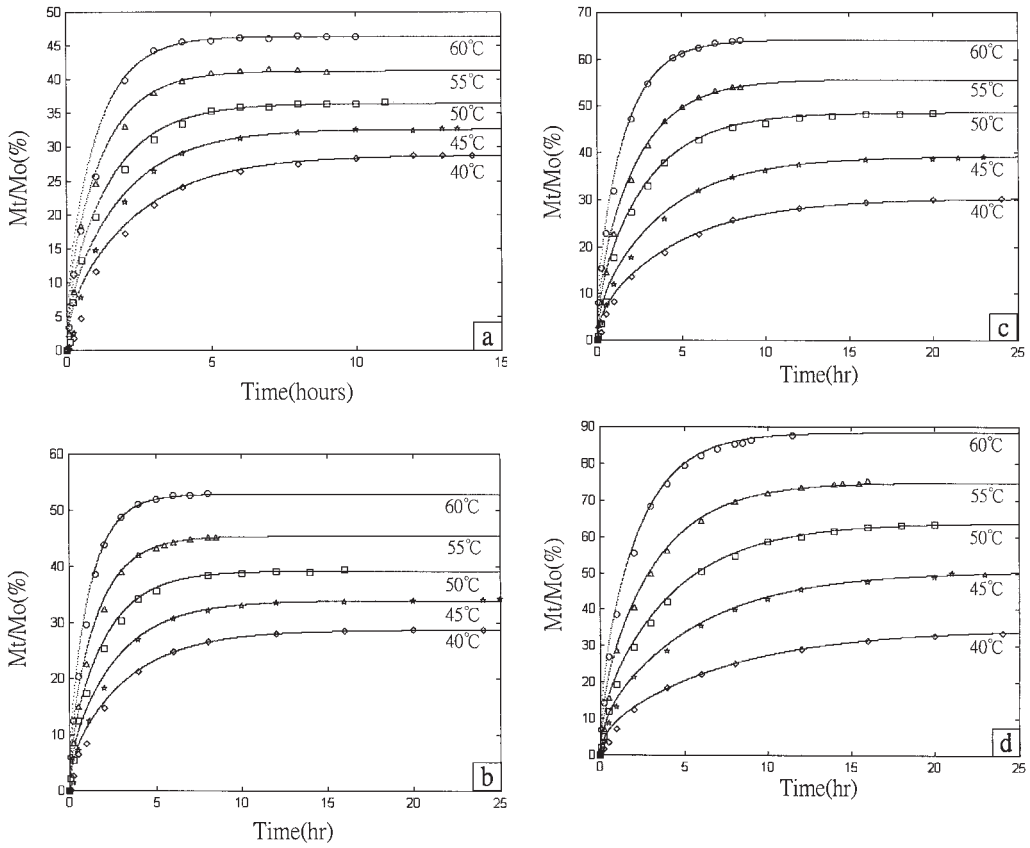

Figure 1 The mass transport of solvent of methanol mixed with various concentrations of $FeCl_3 \cdot 6H_2O$ in PMMA at different temperatures: (a) 0 g/100 g; (b) 2 g/100 g; (c) 5 g/100 g; (d) 8 g/100 g (the rations of $FeCl_3 \cdot 6H_2O$ in methanol).

crystallization-treated. A specimen of 5 × 1 mm thickness was cut and put it in an aluminum pan for the experiment, which used a DSC. The operation temperature of the specimen was measured in the range from 0 to 200°C with a heating rate of 10°C/min and nitrogen flow rate of 30 ml/min.

RESULTS AND DISCUSSION

Mass transport

The experimental data of mass transport for solvent of methanol mixed with different concentrations of $FeCl_3 \cdot 6H_2O$ at 40–60°C are shown in Figure 1, where M_0 is the mass of virgin PMMA prior to solvent mixture treatment. The solid line is a theoretical curve, showing good agreement with the experimental data for solvent with different concentrations of $FeCl_3 \cdot 6H_2O$. It utilizes a mass transport model proposed by Harmon et al.[22,23] The model assumed that the mass transport mechanism accounts for Case I, Case II, and anomalous sorption. The related formula is

$$\frac{M_t}{M_\infty} = 1 - 2\sum_{n=1}^{\infty} \frac{\lambda_n^2(1 - 2\cos\lambda_n)\exp\left(\frac{-vl}{2D}\right)}{\beta_n^4\left(1 - \frac{2D}{vl}\cos^2\lambda_n\right)}\exp\left(-\beta_n^2\frac{Dt}{l^2}\right),$$

where M_t is the weight gain of solvent, M_∞ is the equilibrium weight of the solvent, D is the diffusion coefficient of Case I transport, v is the velocity of Case II transport, $2l$ is the thickness of the specimen, and λ_n is the nth positive root of the equation

$$\lambda_n = \frac{vl}{2D}\tan\lambda_n$$

$$\beta_n^2 = \frac{v^2l^2}{4D^2} + \lambda_n^2.$$

By curve fitting, the values of D and v can be obtained from Figure 1 and are listed in Table I. The values of both D and v decrease with increasing concentration of $FeCl_3 \cdot 6H_2O$ at a given temperature. For various concentrations of $FeCl_3 \cdot 6H_2O$ at 40–60°C, the values of D and v satisfy the Arrhenius equation: $D = D_0\exp(-E_D/RT)$ and $v = v_0\exp(-E_v/RT)$, where D_0 and v_0 are pre-exponent factors. E_D and E_v are activation energies of Case I and Case II transport, respectively. The values of E_D and E_v are calculated using the above Arrhenius equation and are listed in Table II. The activation energy (E_D, E_V) of Case I diffusion and that of Case II diffusion increase with increasing concentration of $FeCl_3 \cdot 6H_2O$.

TABLE I
Diffusion Coefficient (D) for Case I Diffusion, Velocity (v) for Case II Diffusion, and Equilibrium Solvent Content (ESC) in Solvent of Methanol Mixed with Different Concentration of $FeCl_3 \cdot 6H_2O$ at 40–60°C

Temperature (°C)	$FeCl_3 \cdot 6H_2O$/methanol (g/g)	$D\times10^8$ (cm^2/s)	$v\times10^6$ (cm/s)	ESC (%)
60	0/100	18.60	17.50	46.41
	2/100	15.93	15.10	52.81
	5/100	11.90	11.70	64.10
	8/100	8.73	8.11	88.37
55	0/100	16.20	14.71	41.28
	2/100	12.00	10.70	45.35
	5/100	8.20	7.90	55.74
	8/100	6.14	5.13	74.84
50	0/100	12.90	11.68	36.45
	2/100	9.57	8.43	39.15
	5/100	6.66	5.86	48.59
	8/100	4.57	3.73	63.80
45	0/100	10.44	9.70	32.65
	2/100	7.29	6.25	33.85
	5/100	4.93	4.15	39.18
	8/100	3.50	2.90	50.58
40	0/100	8.31	7.90	28.77
	2/100	5.90	4.80	29.43
	5/100	4.00	3.10	30.24
	8/100	2.60	1.87	34.91

The equilibrium solvent content (ESC) is defined as the equilibrium weight of solvent mixture in the specimen (M_∞) divided by the weight of the virgin specimen (M_0). The values of ESC for various concentration of $FeCl_3 \cdot 6H_2O$ at 40–60°C are also listed in Table I. The values of ESC increase with increasing concentration of $FeCl_3 \cdot 6H_2O$ and working temperature. This indicates that the mass transport process is an endothermic reaction. The equilibrium solvent content fits the van't Hoff equation,

$$\mathrm{ESC} = (\mathrm{ESC})_0 \exp\left(\frac{-\Delta H}{RT}\right),$$

where $(ESC)_0$ and ΔH are the pre-exponent factor and heat of mixing, respectively. The values of ΔH for various concentration of $FeCl_3 \cdot 6H_2O$ at 40–60 °C were calculated using the van't Hoff equation and are listed in Table II. The values of ΔH increase with increasing concentration of $FeCl_3 \cdot 6H_2O$ at a given temperature.

TABLE II
Activation Energies of E_D and E_v for Case I and Case II Transport and Heat of Mixing ΔH

	$FeCl_3 \cdot 6H_2O$/methanol (g/g)			
	0/100	2/100	5/100	8/100
E_D(kcal/mol)	1.859	2.248	2.431	2.698
E_v(kcal/mol)	1.817	2.560	2.984	3.174
ΔH(kcal/mol)	1.078	1.322	1.684	2.043

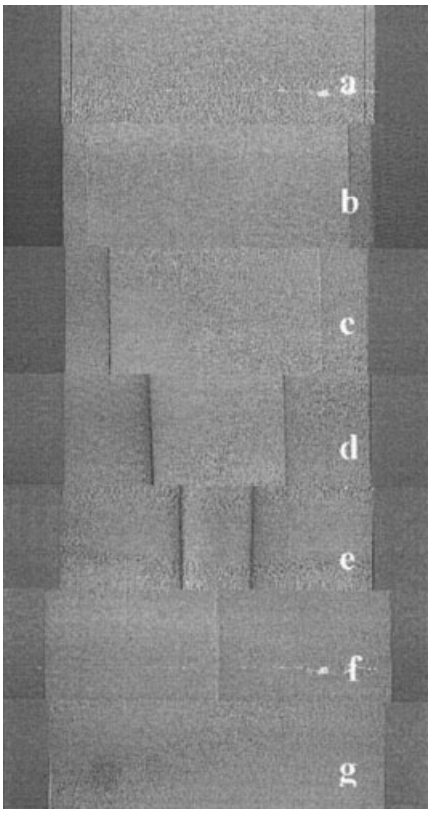

Figure 2 A sequence of photographs for PMMA taken immediately after (a) 30 min; (b) 1 h; (c) 2 h; (d) 4 h; (e) 6 h; (f) 8 h; and (g) 12 h of exposure to solvent of methanol mixed with 2 g/100 g $FeCl_3 \cdot 6H_2O$ at 40°C.

Figure 2 shows a sequence of optical micrographs of the cleavage surface subjected to different times of exposure into solvent of methanol mixed with 2 g/100 g $FeCl_3 \cdot 6H_2O$ at 40°C, exhibiting the sharp boundary or sharp front demarcating the opaque outer region from the transparent inner region, due to the concentration of the solvent mixture being higher in the outer region than in the inner region. Consequently, the effective glass transition temperature ($T_{g,eff}$) is lower in the outer region than in the inner region. After desorption, the holes have relatively more time to grow in the outer region, but cannot easily grow in the inner region.[24] Therefore, the light contrast difference between the outer and inner regions is more obvious. The position of the sharp front as a function of exposure time at different temperatures and solvent of methanol mixed with 2 g/100 g and 5 g/100 g concentrations of ferric chloride hexahydrate are shown in Figure 3. The position of the sharp front increased with increasing exposure time and then slowed down until both sharp fronts meet at the center. The time at which the sharp fronts meet at the center decreased with increasing concentration of $FeCl_3 \cdot 6H_2O$ and working temperature, as shown in Table III.

Crystallization

The cleavage surface of PMMA was immersed into saturated solvent of methanol mixed with 8 g/100 g $FeCl_3 \cdot 6H_2O$ at 60°C, followed by complete desorption in air, and then CO_2 gas was slowly diffused into well-desorbed PMMA for 48 h, as shown in Figure 4. Particulates of about 80 nm average size were precipitated and distributed uniformly in the PMMA matrix. Through XRD diffraction analysis, virgin PMMA showed an amorphous structure with no X-ray peaks and recrystallization-treated PMMA has X-ray peaks from the iron carbonate ($FeCO_3$) phase, as shown in Figure 5, due to ferric chloride hexahydrate as a coordinate compound; in organic solution it forms more than one kind of anionic composite or ion pair, such as $FeCl_4^-$, $FeCl_2S_4^+$, $FeClS_5$, FeS_6^{3+}, and Cl^-[25] (S here indicates molecules of organic solvent). After PMMA absorbed the saturated solvent mixture, these anionic compounds or ion pairs existed in the free volume of PMMA, and then the CO_2 gas slowly diffused into the free volume of the PMMA matrix. The crystallization takes place by way of nucleation and the growth process, and CO_2 gas produces a chemical replacement reaction with these anionic compounds or ion pairs of free volume in the PMMA matrix, resulting in precipitating iron carbonate. Because of a growth boundary loss of concentration of $FeCl_3 \cdot 6H_2O$ within the free volume, the forms size of the iron carbonate particulate to be smaller and even achieves nanoscale. It is worth mentioning that the size of the nano iron carbonate particulates is independent of the concentration of $FeCl_3 \cdot 6H_2O$. Figure 6 shows the relation between the increment ($M_t/M_0 \times 100\%$) of iron carbonate particulates and mass transport time for solvents of methanol mixed with different concentrations of $FeCl_3 \cdot 6H_2O$ at 40 and 60 °C, where M_t is defined as the weight gain of recrystallization-treated PMMA (note that M_t contained about 2% of the residual solvent mixture in the PMMA matrix). The increment of iron carbonate particulates increased with increasing crystallization time until a saturated value was reached. The equilibrium iron carbonate particulate content for the solvent of methanol mixed with different concentrations of $FeCl_3 \cdot 6H_2O$ at 40–60°C is shown in Table IV. The increment of the equilibrium nanoscale iron carbonate particulates increased with increasing working temperature and concentrations of $FeCl_3 \cdot 6H_2O$.

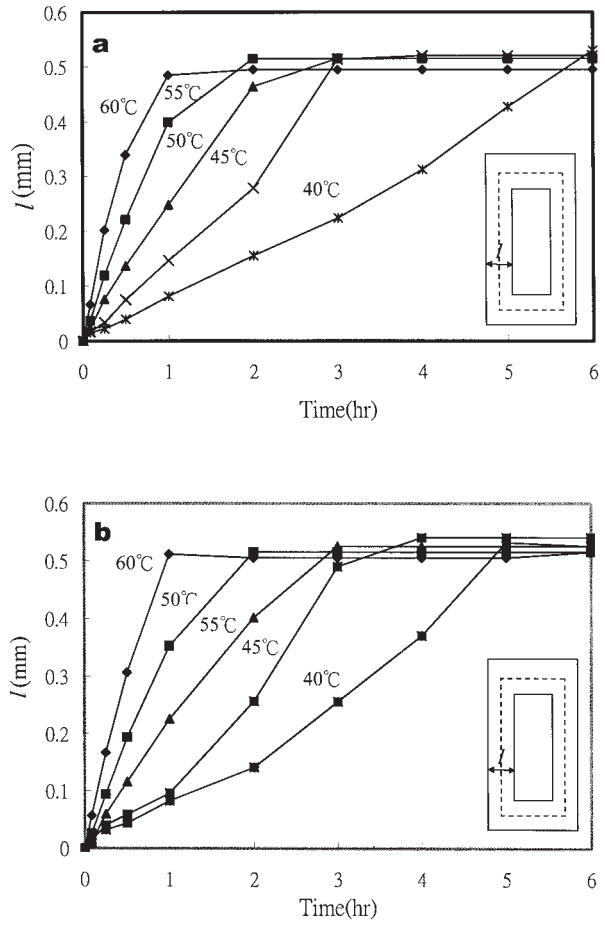

Figure 3 The distance l between the sharp front and the surface as a function of the period of exposure into solvent of methanol mixed with (a) 2 g/100 g and (b) 5 g/100 g $FeCl_3 \cdot 6H_2O$ at different temperatures. The dashed lines in the inset represent the original specimen size.

TABLE III
Time (min) of Sharp Fronts Meeting at the Center Subjected to Solvent of Methanol Mixed with Different Concentrations of $FeCl_3 \cdot 6H_2O$ at 40–60°C

Temperature (°C)	$FeCl_3 \cdot 6H_2O$/methanol (g/g)			
	0/100	2/100	5/100	8/100
40	360	300	288	280
45	258	246	228	204
50	192	180	168	150
55	122	117	108	96
60	72	60	53	51

Transmittance spectrum

The transmittance spectrum of the specimens treated with solvent of methanol mixed with different concentration of $FeCl_3 \cdot 6H_2O$ at 40 and 60°C in the 200- to 850-nm region is shown in Figure 7(a,b). The transmittance of the saturated solvent mixture treated PMMA below the cut-off wavelength is completely absorbed. The transmittance decreased with increasing concentration of $FeCl_3 \cdot 6H_2O$, and its cut-off wavelength moved toward the long wavelength (red shift). According to Chou et al.,[18] after being excited by light, these $FeCl_4^-$, $FeCl_2S_4^+$, $FeClS_5$, FeS_6^{3+}, and Cl^- ion-pairs or anions complexed in the organic solvent show the charge transfer from solvent or ligand to the metal

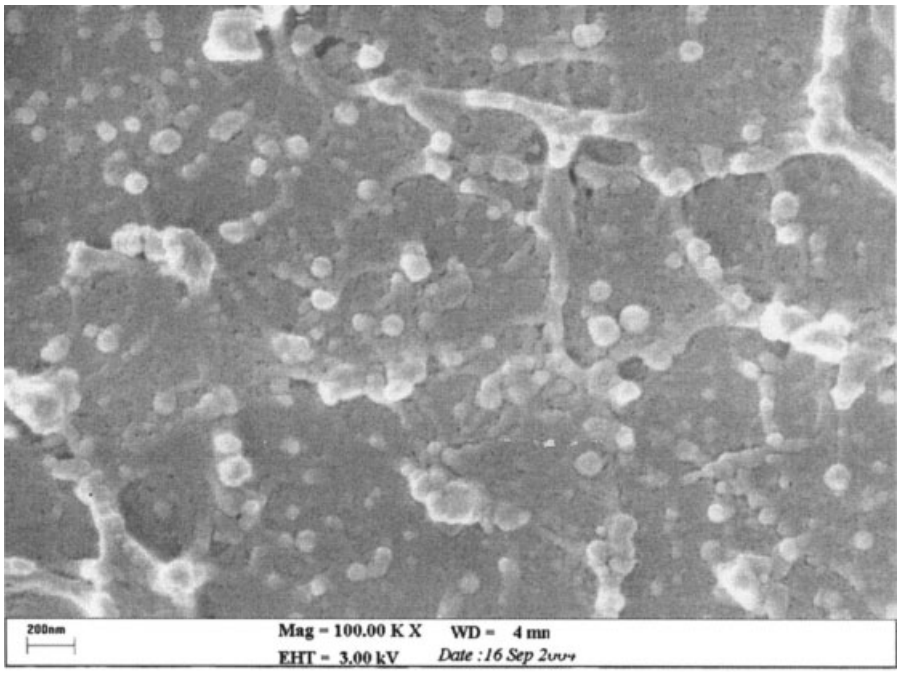

Figure 4 SEM micrographs of PMMA absorped saturated solvent of methanol mixed with 8 g/100 g $FeCl_3 \cdot 6H_2O$ at 60°C and then slowly diffused of supersaturated ammonium carbonate.

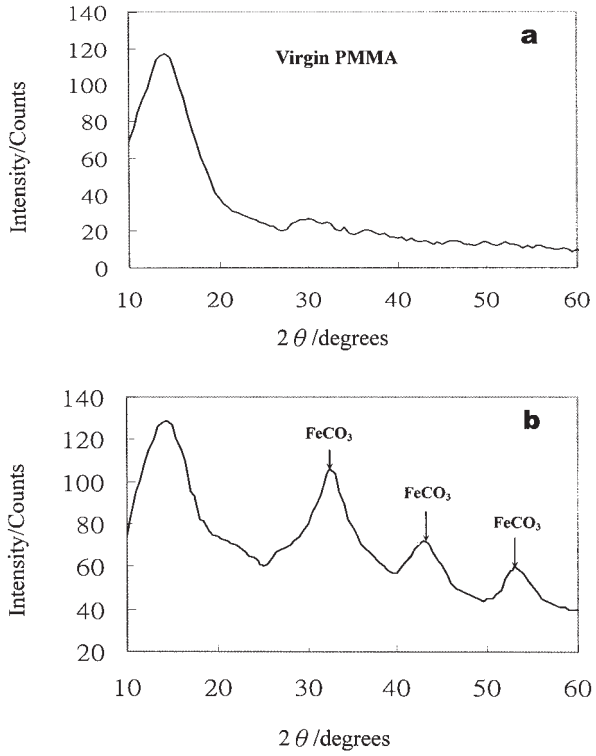

Figure 5 The X-ray diffraction patterns of (a) virgin PMMA and (b) PMMA exposure into solvent of methanol mixed with 8 g/100 g $FeCl_3 \cdot 6H_2O$ at 60°C, and then CO_2 was slowly diffused into PMMA for 48 h.

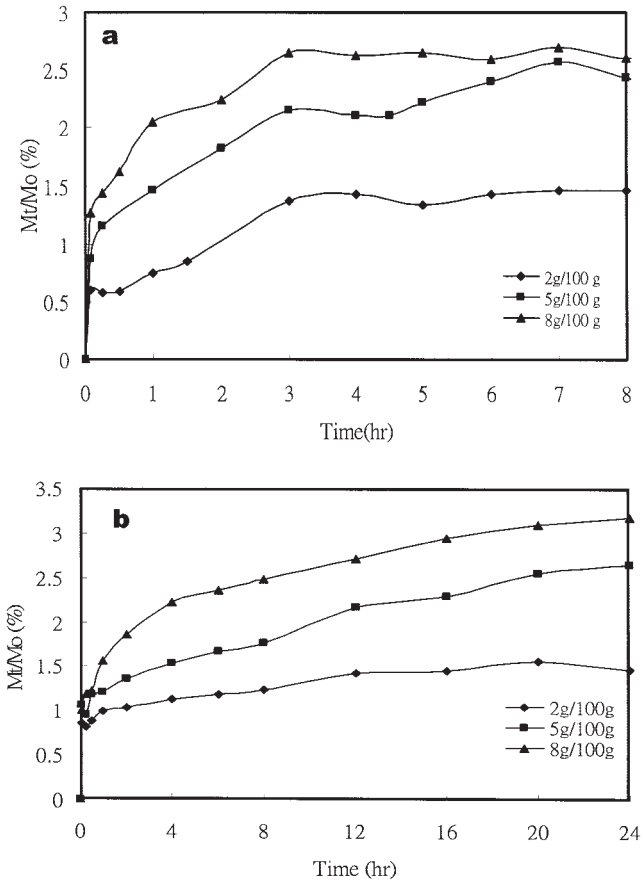

Figure 6 The increment of PMMA after recrystallization treatment at various concentrations of solvent of methanol mixed with $FeCl_3 \cdot 6H_2O$ at different temperatures: (a) 40°C and (b) 60°C, and then slowly diffused of supersaturated ammonium carbonate.

TABLE IV
Equilibrium Iron Carbonate Compound Content (M_t/M_0 × 100%) of Specimens Treated with Solvent Mixture for Various Concentrations of $FeCl_3 \cdot 6H_2O$ at 40–60°C

Temperature (°C)	$FeCl_3 \cdot 6H_2O$/methanol (g/g)		
	2/100	5/100	8/100
40	1.40	2.16	2.53
45	1.43	2.30	2.91
50	1.46	2.61	3.47
55	1.49	3.06	3.83
60	1.51	3.27	4.00

TABLE V
Cut-off Wavelengths (nm) of Saturated Solvent Mixture Treated and Crystallization Treated PMMA

	PMMA					
	Saturated solvent mixture treated (40–60°C)	Crystallization treated				
X(g/g)		40°C	45°C	50°C	55°C	60°C
0	250	250	250	250	250	250
2/100	419	330	353	365	377	403
5/100	456	365	397	400	425	440
8/100	460	452	454	458	460	480

center, in order to oxidize the solvent or ligand and reduce the metal center. As a result, an absorbed optical band induced by the charge transfer was observed. The higher the oxidation state of the metal center, the more easily the charge transfer process occurs. The component with a metal center of high oxidation state is produced in the solvent mixture with high concentration of $FeCl_3 \cdot 6H_2O$, which leads to an absorbed band extending to the range of a longer wavelength.

Figure 7 (c,d) shows the transmittance spectrum of the crystallization-treated specimens (nanocomposites) treated with solvent of methanol mixed with different concentrations of $FeCl_3 \cdot 6H_2O$ at 40 and 60°C in the 200- to 850-nm region. The transmission is apparently lower in the crystallized specimen than in the specimen treated with saturated solvent mixture because the iron carbonate crystals scatter more light than ion pairs and anion complexes and lead to a decrease of transmission. According to Rayleigh,[15] the scattering intensity is proportional to the square of the electric field arising from the particulate, whose size is smaller than the visible wavelength. The electric field due to particulate scattering is inversely proportional

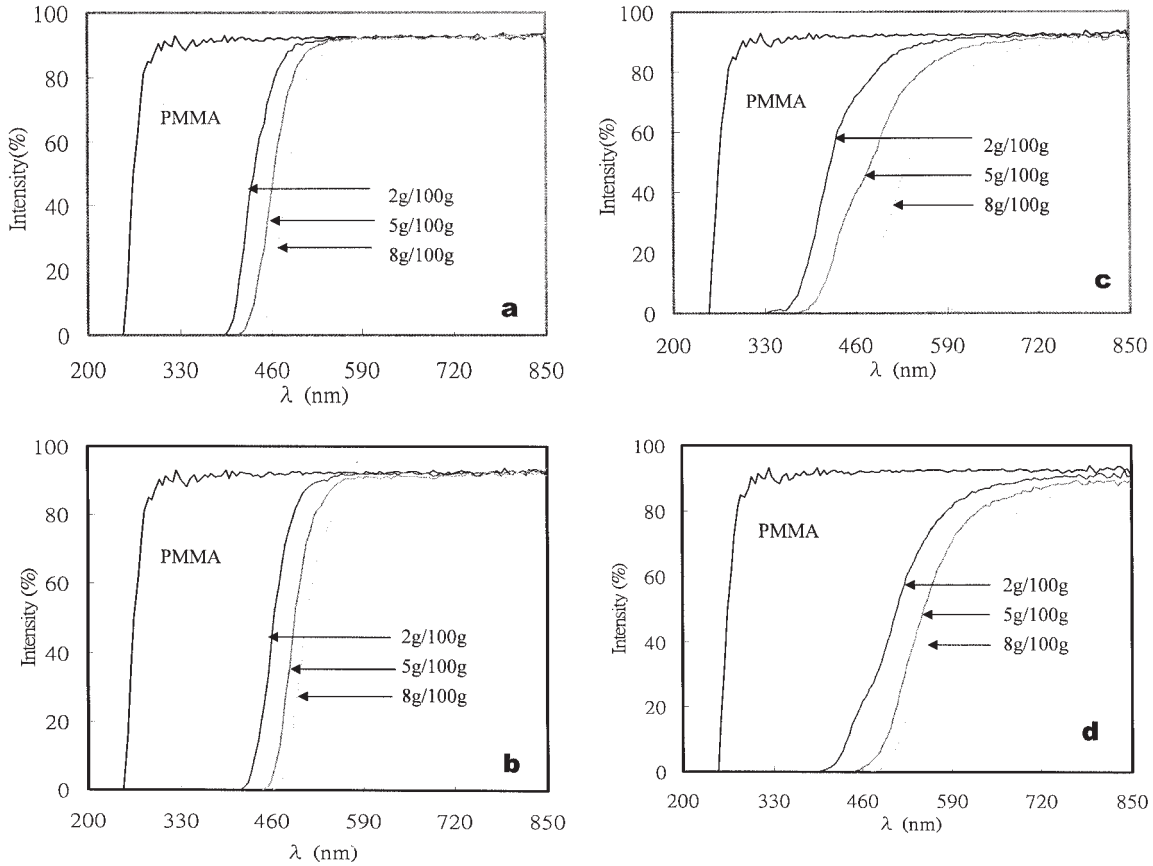

Figure 7 The transmission spectrum of the specimens treated with solvent mixture of different concentration of $FeCl_3 \cdot 6H_2O$ at (a) 40°C and (b) 60°C after desorption; (c) 40°C and (d) 60°C after crystallization treatment.

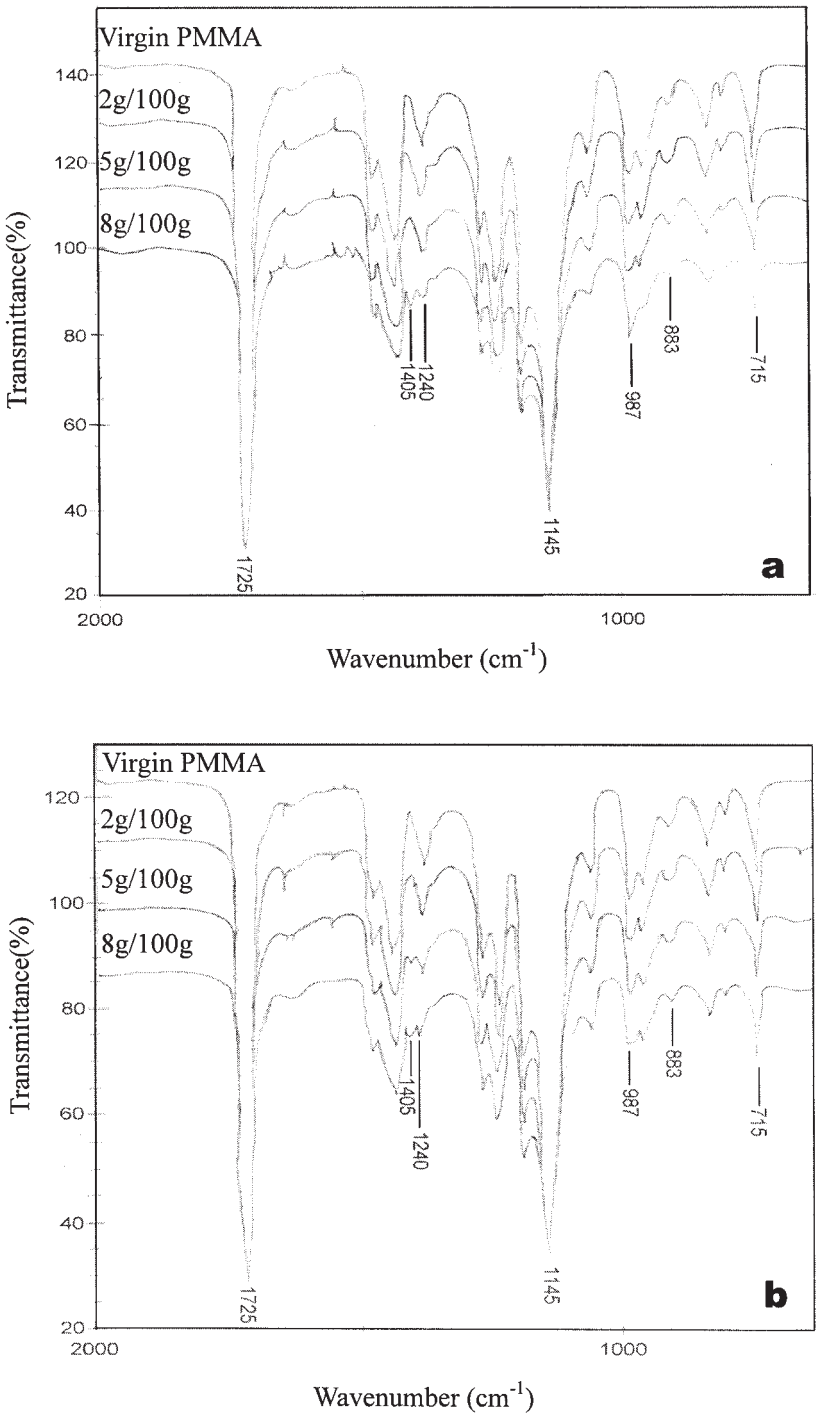

Figure 8 FTIR spectra of (a) solvent mixture treated PMMA and (b) crystallization treated PMMA at 60°C.

to the square of visible wavelength when the surface of the particulates is considered. The surface dimension of the particulate is 2. Thus, the scattering intensity is proportional to λ^{-4}. Rayleigh also suggested that the dependence of scattering intensity upon light wavelength arises from the different obstructive efficiency of the small particulate to various light wavelengths. PMMA is transparent in the visible range, i.e., transmittance is above 90%. For specimens with nanoscale particulates, the dependence of scattering intensity upon visible wavelength is only attributable to the nanoparticulates. Thus, for recrystallization-treated specimens, the relationship between transmittance and light wavelength is influenced not only by the presence of nanoscale particulates but also by the residual ion pairs and anion complexes within the specimen. Further, the cut-off wavelength of the crystallization-treated specimen is shorter than that of the

specimen treated with saturated solvent mixture, as shown in Table V. Thus, higher light energy is required to excite the photoreaction, which causes the absorption band and cuts off at the high-energy band (the range of short wavelength).

Infrared spectrum analysis

Infrared is an analysis methodology to monitor = ion interaction with molecular chains. Figure 8(a) shows the FTIR spectra of virgin PMMA and PMMA with solvent of methanol mixed with different saturated concentrations of $FeCl_3 \cdot 6H_2O$. In the spectrum of virgin PMMA, the C = O symmetrical stretch gives a sharp peak at about 1725 cm^{-1}, asymmetric stretching vibrations of C-O-C bond are identified at about 1240 and about 1145 cm^{-1}, absorption of v (C-O) of the OCH_3 group appears at about 1190 cm^{-1}, and symmetrical stretch of the C-O bond in the C-O-C linkage of PMMA is at about 987 cm^{-1}.[26] By comparing the solvent mixture treated PMMA with virgin PMMA, it can be found that the transmittance intensity of the solvent mixture treated specimen is reduced and no new intense peak is observed, except the one at 60°C and concentration 8 g/100 g of $FeCl_3 \cdot 6H_2O$, which has an obvious extra absorption peak at 1405.06 cm^{-1}.

The PMMA with or without nano iron carbonate particulates had the same peak with no difference except the lower intensity for PMMA with nano iron carbonate as shown in Figure 8 (b). This observation indicates the presence of the nanoscale iron carbonate particulates is not able to enhance the interaction between the PMMA carbonyl and the nanoscale iron carbonate particulates, e.g., the nanoscale iron carbonate crystals do not have primary bonds to molecular chains of PMMA.

Glass transition temperature

Generally, ceramic macrofillers are incorporated into a polymer matrix and therefore do not directly contribute to the glass transition temperature (T_g) of the polymer matrix. Instead, the interaction of the molecule chains with the high specific surface area of the nanofillers can drastically change the molecular chain kinetics in the region immediately surrounding the nanofillers, owing to the presence of the interface. The glass transition temperature of the nanocomposites is shown in Table VI and is larger than that of virgin PMMA (114.4°C), and there is an increment in the glass transition temperature as a function of the amount of nano iron carbonate particulates. That is, a large amount of nano iron carbonate particulates provides an enormous amount of interfacial area and reduces effectively the mobility of molecular chains, resulting in the rising increment of glass transition temperature.

TABLE VI
Glass Transition Temperature of Nanocomposite Preparation in Various Concentrations of $FeCl_3 \cdot 6H_2O$/Methanol (g/g) at 40–60°C

Temperature (°C)	T_g				
$FeCl_3 \cdot 6H_2O$/methanol	40°C	45°C	50°C	55°C	60°C
2 g/100 g	117.3	116.7	115.9	119.6	122.7
5 g/100 g	119.7	120.0	121.4	122.3	124.1
8 g/100 g	121.2	125.1	127.5	129.3	130.2

The glass transition temperature of original PMMA is 114.4°C.

CONCLUSIONS

The conclusions are as follows:

1. The sorption of solvent of methanol mixed with ferric chloride hexahydrate is an anomalous transport and endothermic reaction, and the heat of mixing and equilibrium solvent content increases with increasing concentration of ferric chloride hexahydrate.
2. The activation energy of Case I diffusion and Case II diffusion increases with increasing concentration of ferric chloride hexahydrate.
3. After CO_2 gas was slowly diffused into the PMMA treated with saturated solvent mixture, by way of nucleation and growth process, about 80 nm iron carbonate particulates was precipitated and evenly to distribute in the PMMA matrix. The increment of the equilibrium nanoscale iron carbonate particulates increased with increasing working temperature and concentration of ferric chloride hexahydrate.
4. For the solvent mixture treated PMMA, the transmittance decreased with increasing concentration of ferric chloride hexahydrate, and its cut-off wavelength moved toward the long wavelength (red shift). The transmittance intensity and the cut-off wavelength of nanocomposites are apparently lower than that of the solvent mixture treated PMMA.
5. From FTIR analysis, the spectrum intensity of the solvent mixturetreated PMMA is reduced, and no new intense peak is observed except the one with concentration 8 g/100 g of solvent mixture at 60°C, which has one extra absorption peak at 1405.06 cm^{-1}. Virgin PMMA and nanocomposites had the same peak with no difference except the lower intensity for PMMA with nano iron carbonate.
6. The glass transition temperature of the nanocomposites is higher than that of virgin PMMA and the increment in glass transition temperature as a function of the amount of nano iron carbonate particulates.

References

1. Silberberg, A. Macromolecules 1980, l3, 742.
2. Fujita, H. In Diffusion in Polymers; Crank, J.; Park, G. S.; Eds.; Academic Press: London, 1968; Chapter 3.
3. Hopfenberg, H. B.; Stannett, V. In The Physics of Glassy Polymers; Haward, E. N., Ed.; Wiley: New York, 1973; Chapter 9.
4. Alfrey, T.; Gurnee, E. F.; Lloyd, W. G. J Polym Sci 1966, C12, 249.
5. Hopfenberg, H. B.; Frisch, H. L. J Polym Sci B 1969, 7, 405.
6. Fu, T. Z.; Durning, C. J. AICHE J 1993, 39, 1030.
7. Sarti, G. C. Polymer, 1979, 20, 827.
8. Svorcik, V.; Kozlova, J.; Rybka, V.; Hnatowicz, V. Mater Lett 1995, 23, 321.
9. Kojima, Y.; Usuki, A.; Kawasaki, M.; Fukushima, Y.; Okada, A.; Kurauchi, T.; Kamigaito, O. J Mater Res 1993, 8, 1185.
10. Mano, V.; Felishert, M. I.; Paoli, M. D. Macromolecules 1997, 30, 3026.
11. Bailey, J. K.; Brinker, C. J.; Mecartney, M. L. J Colloid Interface Science 1993, 157, 1.
12. Tawansi, A.; Oraby, H.; Iabdelkader, H.; Abdelaziz, M. J Magn Magn Mater 2003, 262, 203.
13. Tawansi, A.; Zidan, H. M.; Eldumiaty, A. H. Polym Test 1998, 17, 211.
14. Stacey, K. A. In Light-Scattering in Physical Chemistry; Academic Press: New York, 1956.
15. Jenkins, F. A.; White, H. E. In Fundamentals of Optics, 2nd ed.; McGraw–Hill: New York, 1950; Chapter 22.
16. Lin, C. B.; Liu, K. S.; Lee, S. J Polym Sci B Polym Phys 1991, 29, 1457.
17. Chou, K. F.; Lee, S. Polymer 2000, 41, 2059.
18. Orbach, R. Science 1986, 231, 814.
19. Buczkowski, S.; Hildgen, P.; Cartilier, L. Fractals 1998, 6, 171.
20. Wong, P. Z. Phys Rev B 1985, 32, 7417.
21. Wong, P. Z. In Physics and Chemistry of Porous Media; Banavar, J.; Koplik, J.; Winkler, K., Eds.; American Institute of Physics: New York, 1987.
22. Harmon, J. P.; Lee, S.; Li, J. C. M. J Polym Sci A Polym Chem 1987, 25, 3215.
23. Harmon, J. P.; Lee, S.; Li, J. C. M. Polymer 1988, 29, 1221.
24. Lin, C. B.; Liu, K. S.; Lee, S. J Appl Polym Sci 1991, 29, 1457.
25. Drago, R. S.; Har, D. M.; Carlson, R. L. J Am Chem Soc 1965, 87, 1900.
26. Rajendran, S.; Mahendran, O.; Kannan, R. J Phys Chem Solids 2003, 63, 303.